Am J Nucl Med Mol Imaging 2023;13(5):195-207
www.ajnmmi.us /ISSN:2160-8407/ajnmmi0153070

Review Article

Marriage of radiotracers and total-body PET/CT rapid imaging system: current status and clinical advances

Yuxuan Wu[1,2*], Xiaona Sun[1,2*], Boyang Zhang[1,2*], Siqi Zhang[2], Xingkai Wang[2], Zhicheng Sun[1], Ruping Liu[1], Mingrong Zhang[3], Kuan Hu[2,3]

[1]Beijing Engineering Research Center of Printed Electronics, School of Printing and Packaging Engineering, Beijing Institute of Graphic Communication, Beijing 102600, China; [2]State Key Laboratory of Bioactive Substance and Function of Natural Medicines, Institute of Materia Medica, Chinese Academy of Medical Sciences and Peking Union Medical College, Beijing 100050, China; [3]Department of Advanced Nuclear Medicine Sciences, Institute of Quantum Medical Science, National Institutes for Quantum Science and Technology, Chiba 263-8555, Japan. [*]Equal contributors.

Received August 22, 2023; Accepted September 2, 2023; Epub October 20, 2023; Published October 30, 2023

Abstract: Radiotracers and medical imaging equipment are the two main keys to molecular imaging. While radiotracers are of great interest to research and industry, medical imaging equipment technology is blossoming everywhere. Total-body PET/CT (TB-PET/CT) has emerged in response to this trend and is rapidly gaining traction in the fields of clinical oncology, cardiovascular medicine, inflammatory/infectious diseases, and pediatric diseases. In addition, the use of a growing number of radiopharmaceuticals in TB-PET/CT systems has shown promising results. Notably, the distinctive features of TB-PET/CT, such as its ultra-long axial field of view (194 cm), ultra-high sensitivity, and capability for low-dose tracer imaging, have enabled enhanced imaging quality while reducing the radiation dose. The envisioned whole-body dynamic imaging, delayed imaging, personalized disease management, and ultra-fast acquisition for motion correction, among others, are achieved. This review highlights two key factors affecting molecular imaging, describing the rapid imaging effects of radiotracers allowed at low doses on TB-PET/CT and the improvements offered compared to conventional PET/CT.

Keywords: Total-body PET/CT, long axial field of view, radiopharmaceuticals, low dose, high sensitivity

Introduction

After the initial commercial introduction of positron emission tomography (PET) in 1978 [1], the imaging of human functional metabolism at the cellular-molecular level was realized, which has played a major role in noninvasive clinical imaging [2-4]. In the 21st century, PET combined with its contemporaneous computed tomography (CT) technology has an equally unparalleled role in detecting the metabolic functions of the human body [5]. It has a very high clinical sensitivity compared to other imaging techniques and has played a large role in clinical oncology, neurology, and cardiology while helping to develop new drugs [6, 7].

With conventional PET scanners, the axial field of view (FOV) is 15 to 30 cm [3]. The limited axial field of view and the effect of imaging noise limit the study of dynamic imaging [2]. A long axial field of view (LAFOV) PET/CT scanner is clearly the best solution in terms of signal-to-noise ratio (SNR) sensitivity improvement and the time and economic cost of development (**Figure 1**) [2]. The first total-body PET/CT (TB-PET/CT) with a long-axis field of view of 194 cm was successfully created in 2015 with the investment of China United Imaging, the prototype of uExplorer is currently on the market [8]. In 2018, uExplorer completed its first small sample of scientific scans [8], which was approved by the FDA in the same year. Based on this, the Explorer team of scientists designed two updated products: Penn Explorer [9] and Mini Explorer [10]. In addition, the current LAFOV PET/CT imaging instruments include the Biography Vision Quadra system from Siemens [11].

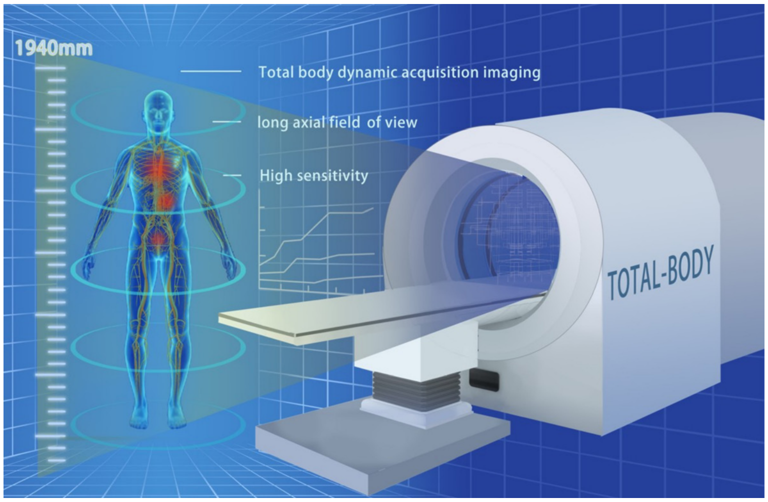

Figure 1. Schematic diagram of TB-PET/CT.

Its technical features include that TB-PET/CT has an extra-long axial field of view and ensures consistent sensitivity over an axial field of view of approximately 1 m at the center, and its 2.9 mm spatial resolution and fused time-of-flight technology achieve better imaging capabilities for small lesions, while the added time dimension allows for 4D panoramic imaging [12]. Its clinical advantages include a TB-PET/CT scanner with increased axial coverage, which improves the sensitivity of imaging, reduces the conventional PET imaging time from 10-20 mins to less than 40 s, reduces the radiation dose while improving the imaging quality, and achieves total-body dynamic imaging [13, 14].

^{18}F-FDG in TB-PET/CT

^{18}F-FDG (**Figure 2A**), the most commonly used radiographic agent in clinical practice, is a glucose analog that accurately reflects glucose metabolism levels in organs/tissues in the body [15]. The relatively hypoxic environment of cancerous tissues requires ten times more glucose for cellular metabolism than normal cells [16]. Therefore, ^{18}F-FDG will be heavily concentrated in the malignant tumor area and make the radioactive intensity in the tumor area significantly different from that in normal tissue.

Although FDG-PET/CT has the potential for non-invasive, precise medical imaging, it still suffers from false-negative detection and inefficient detection of photons emitted by the radiotracer [17-20]. The difficulty of detecting osteogenic metastases due to low levels of glucose metabolism in osteogenic metastases was identified as early as 1998 [17]. Examples include Cook's report of 23 false-negative PET-CT cases of bone metastases in patients with breast cancer [17] and An's report of a false-negative PET-CT case of bone metastases in a patient with non-small cell lung cancer [19].

LAFOV PET can improve the sensitivity of PET scans by covering the entire body. Compared to conventional PET scanners, LAFOV PET can be 10 to 40 times more sensitive, thus enabling the detection of small, low-density tumor deposits (micrometastases) [8, 12, 21, 22]. The first application of TB-PET/CT was quantitatively evaluated in four subjects using decreasing doses of the tracer ^{18}F-FDG (4.5 MBq/kg, 4.5 MBq/kg, 1.35 MBq/kg, 0.45 MBq/kg) for possible imaging improvements with TB-PET/CT. Subject 1 illustrated the feasibility of faster and better imaging, with images of diagnostic quality in 37.5 seconds, good detectability of small lesions in 20 minutes, and low image noise (**Figure 2B**). Subject 2 illustrated the feasibility of later imaging, with imaging images still of diagnostic quality 10 hours after injection, and their repeat scans demonstrated the feasibility of high temporal resolution whole-body dynamic image production. Subject 3 illustrates that single-organ distal imaging with low-dose injection still has a good SNR. The hypothesis of TB-PET/CT was initially verified by the tracer ^{18}F-FDG. The clinical advantages of TB-PET/CT include improved image quality, rapid scanning, multiple post half-life delayed scanning, low-dose scanning, and whole-body pharmacokinetic imaging [8].

Applications in cancer

Modern medical advances have prolonged the life span of patients with chronic malignancies, and the emergence of dynamic imaging with TB-PET/CT scans will also help in personalized and precise treatment as well as side effect management. TB-PET/CT often allows for half-

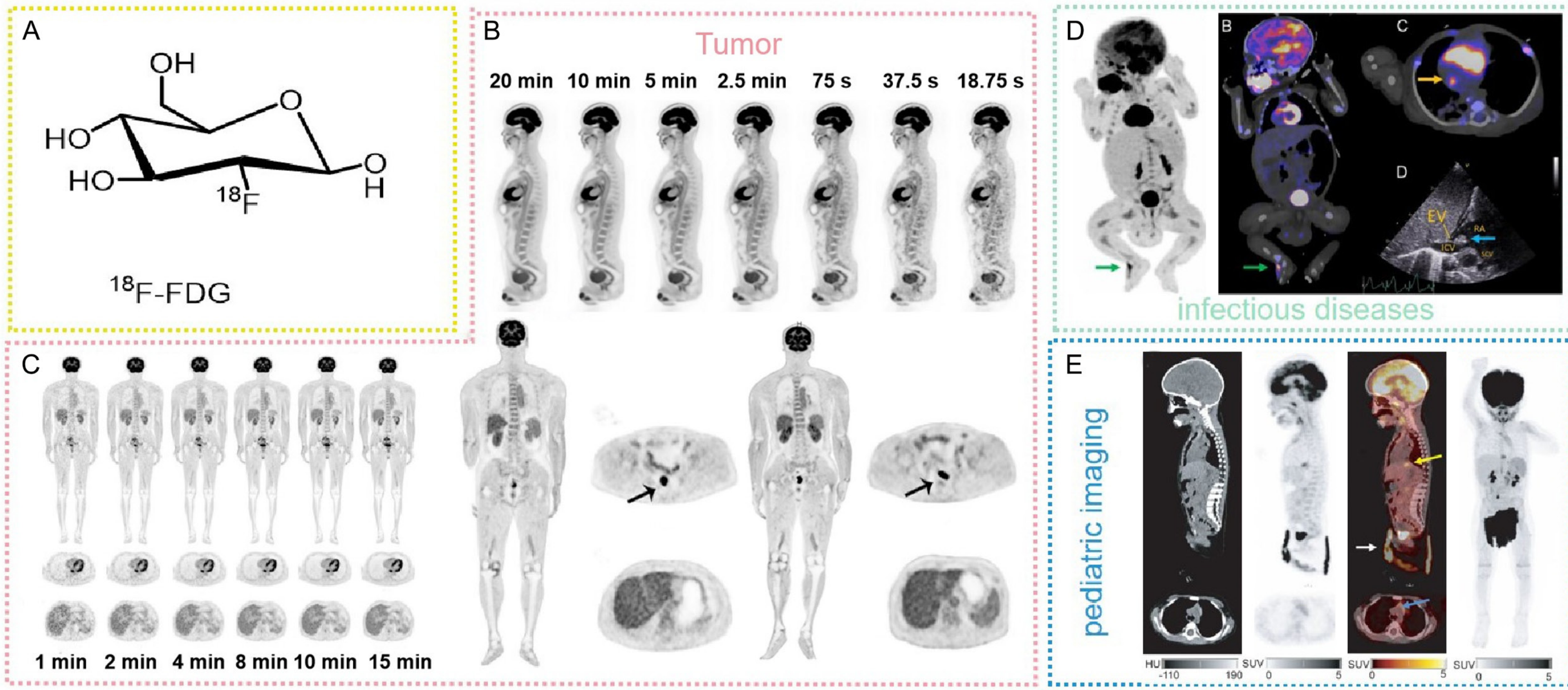

Figure 2. Structure and application of ^{18}F-FDG, a nonspecific tracer. Structural formula of ^{18}F-FDG (A). First clinical application of TB-PET/CT, the imaging quality of a patient over 7 scans (B). PET images of a 63-year-old patient with esophageal cancer at 1 min, 2 mins, 4 mins, 8 mins, 10 mins, and 15 mins (left), where the imaging quality at 2 mins is equivalent to that at 8 mins (right) (C). Staphylococcus aureus infection was detected by TB-PET/CT imaging at the dorsum of the right foot and the entrance to the inferior vena cava (D). Biograph Vision Quadra System 120 s acquisition of CT, PET, PET/CT, and maximum-intensity-projection reconstruction (from left to right) ^{18}F-FDG was not pathologically uptaken, and the arrow in the figure indicates partially reactive aggregation (E). Images reprinted from [8, 26, 29, 32] with permission.

dose whole-body imaging, reducing the radiation dose while improving imaging quality. Tan *et al*. compared half-dose ^{18}F-FDG (1.85 MBq/kg) TB-PET/CT and clinical routine full-dose ^{18}F-FDG PET/CT lung cancer image quality in a group including 56 patients with primary lung cancer, and the image quality score was significantly higher in the half-dose group (4.3±0.7) than in the full-dose group (3.7±0.6) (P=0.004) [23]. Based on previous studies, Sachpekidis *et al*. determined the appropriate acquisition time range for LAFOV Biograph Vision Quadra PET/CT by a low dose (2 MBq/kg) in 49 patients with melanoma, ultimately reducing the conventional acquisition time (10 mins) to 5 mins without affecting the liver SNR and tumor-background ratio (TBR) [24].

In PET/CT, diagnostic imaging quality is not only related to tracer dose, but image quality and noise level are also negatively correlated with acquisition time. Hu *et al*. performed a diagnostic evaluation of ^{18}F-FDG TB-PET/CT (uExplorer) with fast 2-min acquisition versus conventional ^{18}F-FDG-PET/CT (uMI780) in 156 patients with hepatocellular carcinoma divided equally into two groups. The imaging quality of TB-PET/CT in the naked eye was the same at 2 mins and 15 mins. In addition, the cancer detection efficiency of TB-PET/CT imaging with 2 mins rapid acquisition was similar to that of conventional PET/CT [25]. They also performed total-body imaging with low-dose ^{18}F-FDG (0.37 MBq/kg) in 30 tumor patients. Based on the above experience with rapid imaging, a full-dose 2 minutes imaging control group was established in this experiment. Low-dose 8 mins imaging results were of comparable quality to the control group and had acceptable medical diagnostic value (**Figure 2C**) [26]. Zhang *et al*. explored the image value of a more rapid TB-PET/CT scan, comparing 300-second data with 30-second data from TB-PET/CT after injection at a conventional dose (3.7 MBq/kg). Through the analysis of 110 lesions in 84 patients, although the 300-second data had higher sensitivity and accuracy than the 30-second data, the TB-PET/CT images obtained by the 30-second acquisition time reached the diagnostic level of traditional PET/CT. For patients with malignant tumors that cannot be located for a long time, 30-second rapid whole-body PET/CT meets the clinical diagnostic requirements [27].

Applications in infectious diseases

After entering the body, the radiotracer ^{18}F-FDG is taken up preferentially by macrophages and inflammatory cells in tissues. Therefore, ^{18}F-FDG has become the pillar of molecular imaging for infectious diseases (fungal, bacterial, and viral infections) [28]. Traditional ^{18}F-FDG-PET imaging strategies are limited in the therapeutic diagnosis of infectious diseases in the context of complications. TB-PET/CT imaging has emerged in recent years with high sensitivity and the ability to detect low-level signals from background noise. Therefore, new ^{18}F-FDG TB-PET/CT strategies will be at the forefront of clinical and pathogenesis research in infectious diseases [28].

Rijsewijk *et al*. performed TB-PET/CT imaging using an ultra-low dose of ^{18}F-FDG in a 10-week-old neonate with S. aureus sepsis, and the scan identified 2 foci of infection, one on the dorsum of the right foot near the venous access and the other on the base of the right atrium at the entrance to the inferior vena cava, and post-sampling confirmed the foot lesion as Staphylococcus aureus infection (**Figure 2D**) [29]. This case also confirmed the ability of low-dose ^{18}F-FDG TB-PET/CT to image infectious diseases. Chronic (and acute) viral infections such as HIV have been experienced with PET imaging for decades. Since the beginning of the COVID-19 pandemic, the study of infectious diseases in PET imaging has received further attention. Conventional PET/CT is limited by its sensitivity and low SNR, making the study of the pathogenesis of infectious diseases missing as well as false-negative scans in patients with clinical mild infections and small lesions [3].

Applications in pediatric imaging

The first consideration in pediatric PET imaging is the dose of radiopharmaceuticals to be used, as children have higher tissue radiosensitivity and longer life expectancy than adults [30, 31]. LAFOV PET/CT's fast scans and low-dose imaging can help reduce the radiation dose in children [32].

Chen *et al*. summarized 100 pediatric tumor patients receiving half a dose of ^{18}F-FDG (1.85

MBq/kg) using uExplorer imaging to reconstruct PET images at a complete 600-second time. The imaging quality of 300 s, 180 s, 60 s, 40 s, and 20 s was compared, and sufficient image quality and clear lesions could be obtained at a fast scan time of 60 seconds and half-dose activity [31]. A study by Zhao *et al*. found that optimal image quality was achieved with TB-PET/CT by reducing the dose given to 1/10th of the dose (0.37 MBq/kg) [33]. Reichkendler *et al*. imaged a 17-month-old girl with suspected malignancy or focal infection after left heminephrectomy with TB-PET/CT using the Biograph Vision Quadra system. The results of diagnostic value were obtained without the use of sedation, and malignancy or focal infection was ruled out based on the imaging results (**Figure 2E**) [32]. Li *et al*. performed uExplorer PET/CT total-body dynamic scanning using a half-dose tracer ^{18}F-FDG (0.05 mCi/kg) in a sedation-free child to reduce the acquisition time without affecting the image quality even in the presence of involuntary movements of the child [34]. The above examples demonstrate the advantages of long-axis PET/CT in pediatric imaging, allowing for low-dose, high-quality imaging while reducing motion artifacts and avoiding anesthesia.

Specific tracers in TB-PET/CT

Application in prostate cancer-PSMA

Prostate cancer (PC) is the third most common cause of cancer-related death among men worldwide [35, 36]. Given the limitations of other PET radiopharmaceuticals, there is increasing research on radiotracers based on targeting prostate-specific membrane antigen (PSMA) [35]. At present, the most commonly used tracers for PET imaging are ^{68}Ga-PSMA-11 (1, **Figure 3**) [37-40], and ^{18}F-PSMA-1007 (2, **Figure 3**) [41-44]. However, these are all studies based on conventional imaging, in contrast to TB PET/CT, which has advantages such as high sensitivity, large dynamic range, and high image quality. Therefore, Alberts *et al.* injected ^{18}F-FDG, ^{18}F-PSMA-1007, or ^{68}Ga-DOTATOC and performed double scans in 44 patients [45]. The performance of the LAFOV Biograph Vision Quadra PET/CT and the standard axial field of view (SAFOV) Biograph Vision 600 PET/CT system was studied. The results showed that LAFOV captured the same range of integrated activity as SAFOV. In clinical conditions, the LAFOV system has higher sensitivity, with improvements in image quality, lesion quantification, and SNR. Compared to conventional SAFOV acquisition (equivalent to 16 mins of FOV coverage), the LAFOV system can provide images of comparable quality and quantification of lesions within 2 mins.

Imaging 1 h after injection of ^{68}Ga-PSMA-11 is the conventional imaging acquisition time, but this is not the optimal imaging time choice [46, 47]. Although the acquisition of images after a longer acquisition time can improve lesion uptake and contrast, there are many limitations, such as the decay of the short half-life (68 mins) during later imaging and the reduced availability of the scanner due to the longer acquisition time [48]. With the advent of a large dynamic range and highly sensitive LAFOV scanners, late imaging of radiopharmaceuticals can be effectively tracked [2]. Alberts *et al.* studied standard imaging at 1 h and late imaging at 4 h in 10 patients after injection of ^{68}Ga-PSMA-11 [49]. The results showed that the average tumor to the background of 4 h was higher and the SNR was improved compared with 1 h. This suggested that a later acquisition time may be better when using LAFOV for ^{68}Ga-PSMA-11 imaging.

In addition to effectively tracking late imaging, TB imaging PET/CT can also determine the optimal time for prostate cancer ^{68}Ga-PSMA PET/CT imaging. Wen *et al.* studied the time-activity curves of pathological lesions of tumors and physiological bladder activity using TB-PET in 11 patients and determined the optimal imaging time [50]. The study showed that early assessment of pathological lesions with dynamic ^{68}Ga-PSMA PET could avoid interference with bladder activity. However, compared to imaging at 60 mins, early imaging may miss lesions with low PSMA uptake. Looking at the above factors, combining the first 6 minutes of early dynamic imaging with later static imaging can better detect lesions masked by bladder activity and lesions with relatively low PSMA uptake. In addition, they found that ^{68}Ga-PSMA PET imaging can also be performed 35-59 minutes after injection to reduce the wait time for imaging. They also studied the mean SUV values of the lesion and metastasis at 180 mins of delayed imaging and found that they were

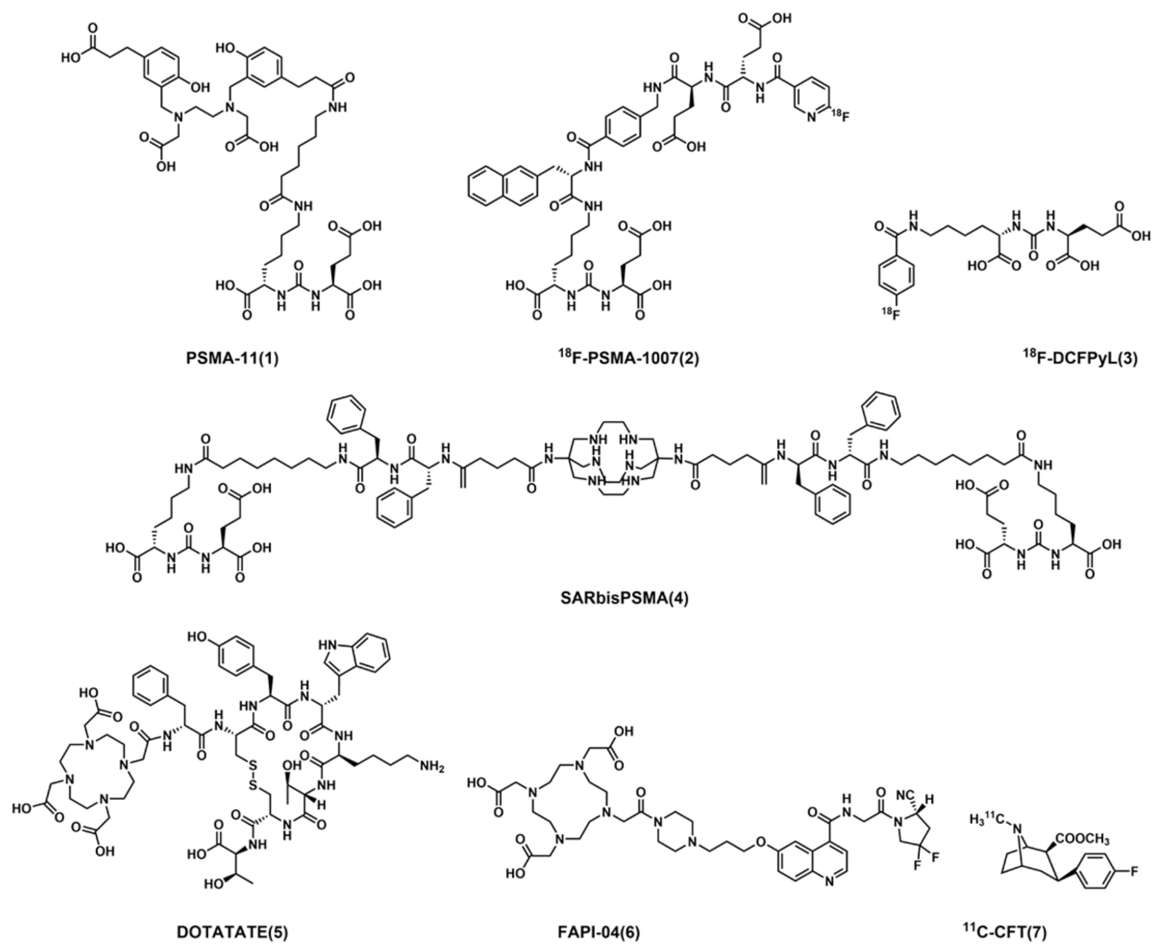

Figure 3. Chemical structure of tracers.

higher than those at 35 mins and 60 mins, indicating that delayed imaging can also satisfy the needs of clinical diagnosis.

The addition of additional 2-^{18}F-FDG PET/CT with higher sensitivity compared to the single PSMA tracer PET/CT can help detect lesions with low expression [51]. Based on this, Alberts *et al.* used the LOFOV PET/CT system to perform ^{68}Ga-PSMA-11 and an additional low-dose 2-^{18}F-FDG PET/CT scan on 14 patients who were to undergo PSMA radioligand therapy examination [52]. The results of the study showed that one in 14 patients (7%) had other lesions with low or absent PSMA expression but high FDG affinity. This demonstrated that additional low doses of 2-^{18}F-FDG-PET/CT can be used as part of the efficacy evaluation of ^{177}Lu-PSMA radioligand therapy, helping to reveal lesions with low PSMA affinity (**Figure 4**) [52].

Specifically, targeted tracers allow for high uptake at the target site and rapid clearance at the injection site. The application of specifically targeted tracers to TB-PET/CT enables the staging of cancer patients and supports personalized patient treatment. For prostate cancer, it is mentioned here that two specific radiotracers with safety and efficacy, ^{18}F-DCFPyL (3, **Figure 3**) and ^{64}Cu-SARbisPSMA (4, **Figure 3**), can be used for TB-PET/CT imaging. ^{18}F-DCFPyL is a radiolabeled, highly selective small molecule PET tracer targeting the membrane protein PSMA, which has good pharmacokinetic properties and is capable of detecting a large number of metastatic suspicious lesions in prostate cancer [53]. ^{64}Cu-SARbisPSMA has now completed a phase I clinical study (NCT04839367) to demonstrate its tolerability and safety [54].

TB-PET/CT enables early visualization of tracer kinetics, based on which more valuable radio-

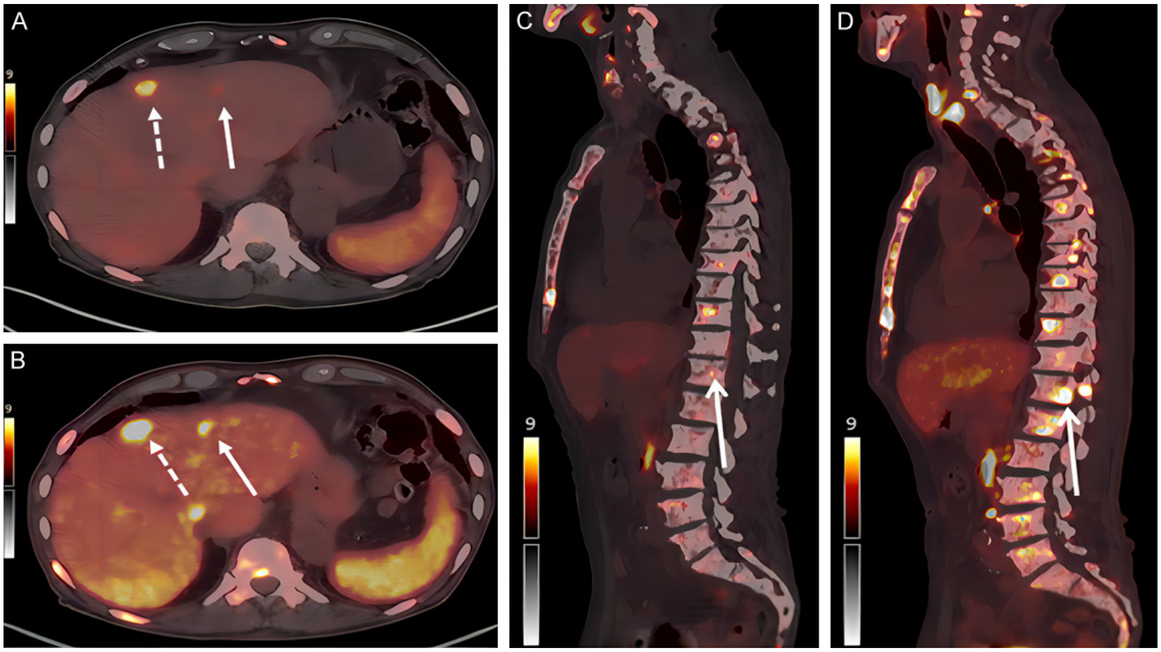

Figure 4. (A, C) show ^{68}Ga-PSMA-11 PET/CT and (B, D) show additional PET/CT performed 1 h after additional FDG administration. Images reprinted from [52] with permission.

tracers can be screened. Ingbritsen *et al.* sequentially injected ^{18}F-DCFPyL (1.2 MBq/kg) and ^{64}Cu-SARbisPSMA (1.66 MBq/kg) in a 69-year-old male patient with prostate cancer restaging to detect angiomyolipoma, followed by dynamic imaging and delayed imaging by the Biograph Vision Quadra system, and ^{18}F-FDGTB-PET/CT scans were performed a few days later [55]. Both ^{18}F-DCFPyL and ^{64}Cu-SARbisPSMA showed good lesion uptake compared to ^{18}F-FDG. Imaging comparisons at 1 h after injection showed higher ^{64}Cu-SARbis-PSMA blood pool activity than ^{18}F-DCFPyL, and ^{64}Cu-SARbisPSMA remained more radioactively retained at 6 h and 30 h in ribs and angiolipomas [55].

Application in neuroendocrine tumor-^{68}Ga-DOTATATE

Neuroendocrine tumors are a heterogeneous group of tumors whose main hallmark is the expression of somatostatin receptor 2 (SSTR2) [56]. PET imaging of ^{68}Ga-DOTATATE (5, **Figure 3**) showed a particularly high binding affinity (0.2±0.04 nM) to SSTR2-positive tissues [57]. In terms of dosing, the recommended dosing activity for ^{68}Ga-DOTA-conjugated peptides was between 100 and 200 MBq, and at least 100 MBq was required to obtain good image quality. In addition, the sensitivity of the PET detector and the patient's weight also affect the injection activity [58]. The TB PET detector with ultra-high sensitivity can achieve good image quality with low doses of tracers. Based on this, Shi's group found that low injected ^{18}F-FDG activity was sufficient to obtain good image quality and did not reduce the detection efficiency of lung cancer [23]. In addition, TB PET detectors can significantly shorten the tracer acquisition time of conventional doses within 2 mins to obtain adequate ^{18}F-FDG PET/CT image quality [59].

Based on the results, their group investigated the feasibility of receiving a low injection dose of ^{68}Ga-DOTATATE TB PET/CT examination in 57 neuroendocrine tumor patients [60]. The results showed that good subjective image quality can be obtained within a 3 mins acquisition time. This suggested that a low dose of ^{68}Ga-DOTATATE TB PET/CT not only reduces acquisition time but also maintains adequate image quality for patients with neuroendocrine tumors.

Application in urothelial carcinoma-^{68}Ga-N188

Nectin cell adhesion molecule 4 (nectin-4) is limited in expression in most normal tissues

[61, 62]. In urothelial carcinoma, it is present in more than 80% of tumor samples and is an emerging biomarker for the diagnosis and treatment of tumors [61]. Duan *et al.* designed a bicyclic peptide radiotracer, ^{68}Ga-N188, targeting nectin-4 and used uExplorer TB-PET/CT for the first clinical evaluation on patients with advanced uroepithelial cancer [63]. Based on the dynamic imaging results from 3 patients with different nectin-4 expression levels, they found that the uptake of nectin-4-positive lesions was obvious at 600 s and 2400 s, while the uptake of nectin-4-negative lesions was less obvious. In addition, from the time distribution results of full dynamic imaging, nectin-4-positive lesions reached the maximum uptake value in approximately 14 mins. The results showed that ^{68}Ga-N188 had a high affinity for nectin-4, and TB PET/CT allowed for faster maximum imaging.

Application in pancreatic and gastric cancer-^{68}Ga-FAPI-04

Fibroblast activation protein (FAP) is an ideal diagnostic and therapeutic target for malignant tumors [64-66]. ^{68}Ga-FAPI-04 (6, **Figure 3**) is a radioactive tracer that targets FAP and can specifically identify tumor cells [67-69]. Long-axis PET/CT enables dynamic whole-body imaging compared to short-axis PET/CT used in previous clinical studies. Shorten the imaging time could achieve multi-parameter imaging from ^{68}Ga-FAPI-04 PET. Therefore, Chen *et al.* studied the feasibility and superiority of ^{68}Ga-FAPI-04 PET imaging versus conventional SUV imaging in 13 patients [70]. They performed image analysis of the kinetic parameters of the two-tissue reversible compartment model (2T4K) and the multigraph models. The results showed that the TB imaging results of ^{68}Ga-FAPI-04 PET were better in the SUV, and the lesion contrast was enhanced. Both V_T (2T4K) images and V_T (Logan with spatial constraint (SC)) images showed lower image noise and higher lesion significance than SUV images. Compared with conventional short axis PET/CT, PET/CT can be used for dynamic total-body imaging of TB. Rhythm spatial synchronization makes it feasible for parametric imaging.

Application in Parkinson's disease-^{11}C-CFT

^{11}C-2-beta-carbomethoxy-3-beta-(4-fluorophenyl) tropane (^{11}C-CFT) (7, **Figure 3**) is a radiolabeled cocaine derivative that binds specifically to dopamine transporters located at the synapses of the anterior membrane in the brain [71]. It is used in the diagnosis of Parkinson's disease. Commonly used ^{18}F-FDG for PET/CT imaging of cerebral glucose metabolism does not specifically distinguish atypical Parkinson's syndrome in brain diagnosis. ^{11}C-CFT with specific binding to brain dopamine transporter PET imaging is symmetrically distributed in the striatum bilaterally in normal subjects and is differentially reduced in patients with Parkinson's disease [71]. However, the short half-life of ^{11}C (20.4 mins) and the incomplete understanding of its human biodistribution limit its clinical application.

TB-PET/CT, which allows whole-body dynamic scanning and enables fast imaging, will help ^{11}C-CFT for the diagnosis of Parkinson's disease and increase the understanding of the human biodistribution of radiotracers. Xin *et al*. injected 373.3±71.56 MBq of ^{11}C-CFT tracer in six male patients suspected of Parkinson's disease, followed by dynamic TB-PET/CT using uExplorer, and a 75-minute PET scan described the biodistribution in PD patients in real time (**Figure 5**) [72]. Tracer uptake and metabolism are rapid in the kidneys, lungs, spleen, and thyroid, with rapid uptake and slow metabolism in the heart wall, slow uptake and metabolism in the liver, and generally low uptake in the brain and muscle, resulting in "low-level extension". Meanwhile, the effective dose of ^{11}C-CFT TB-PET/CT is 2.83E-03 mSv/MBq, a two-thirds reduction in dose compared to conventional multi-bed PET/CT scanning technology [72]. This example demonstrates the value of ^{11}C-CFT in TB-PET/CT imaging of Parkinson's disease by demonstrating good whole-body biodistribution, a very low injection dose, and high imaging quality.

Application in cancer immunotherapy monitoring-^{89}Zr-trastuzumab

^{89}Zr-labeled antibodies represent promising reagents for cancer immunotherapy monitoring. Several of these radiopharmaceuticals have already been utilized in clinical settings, such as ^{89}Zr-atuzumab, ^{89}Zr-anti-CD8 microantibodies, and ^{89}Zr-trastuzumab [73-76]. However, most currently available commercial scanners lack a sufficient SNR for image reconstruc-

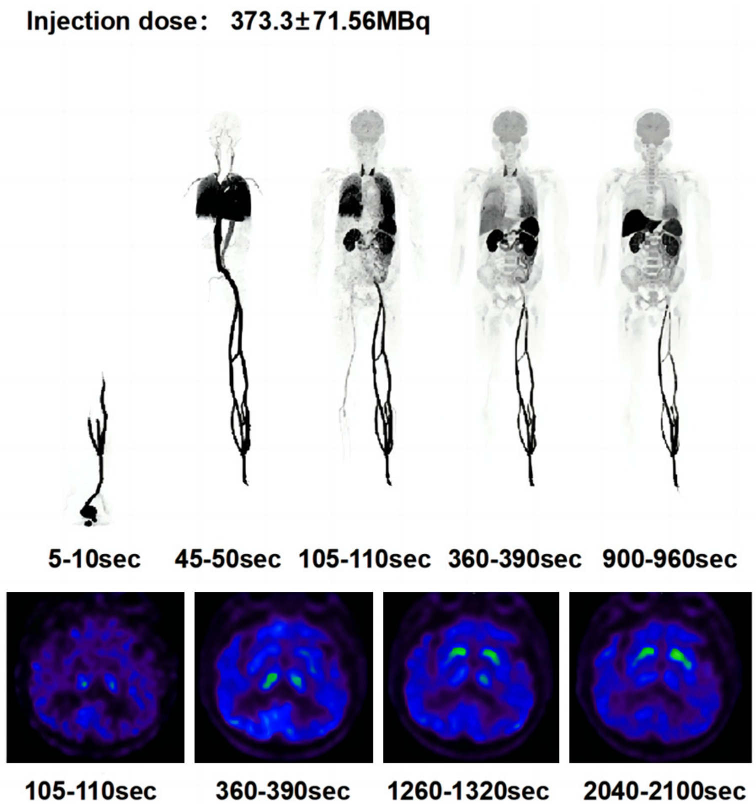

Figure 5. TB-PET/CT imaging results of a Parkinson's patient showing ^{11}C-CFT at five time points of body circulation (top) as well as four nodes of brain uptake (bottom). Images reprinted from [72] with permission.

tion and accurate interpretation and quantification within the 2-3 physical half-life (25 s) range [22]. Consequently, extending PET imaging beyond 7-10 days post-injection with acceptable radiation exposure remains challenging, even for ^{89}Zr, a positron emission isotope with a long half-life [77].

Berg *et al.* demonstrated the feasibility of extending the ^{89}Zr-PET study up to 30 days post-injection using the high-sensitivity primate Mini Explorer PET system. In a study involving 12 young rhesus macaques, the pharmacokinetics of four Zr chelator linkers associated with humanized IgG antibodies were evaluated. Through quantitative image analysis of differential bone and liver uptake at later time points using total-body PET/CT, enhanced stability of the ^{89}Zr chelator was achieved using the octacectaate chelator DFO*. Even at very late time points, remarkable agreement was observed within each group, enabling the observation of variations in tissue and bone uptake of different chelators and linkers [78].

Conclusions

The utilization of long-axis PET/CT in clinical practice has demonstrated its ability to achieve high-quality imaging with a low-dose radiotracer, due to its ultra-high sensitivity and SNR. This advancement has paved the way for various clinical applications including whole-body dynamic imaging, delayed imaging, personalized disease management, and ultrafast acquisition for precise motion correction. The development of the TB-PET/CT system has further expanded its capabilities by enabling delayed imaging and multiple repeat imaging. Because of the delayed imaging capability of TB-PET/CT, allows for the meaningful utilization of longer half-life radionuclides and introduces new possibilities with long-lived radionuclides. Although the availability of TB-PET/CT imaging systems is currently limited to a few institutions, the existing imaging results have already demonstrated the superiority of TB-PET/CT over conventional imaging methods. As long-axis imaging systems continue to gain wider usage and a broader range of radiopharmaceuticals are incorporated, LAFOV PET/CT has the potential to not only aid in disease identification but also greatly contribute to drug development, disease follow-up, screening of high-risk populations, and other yet unimagined applications.

Acknowledgements

This study was supported by the Nonprofit Central Research Institute Fund of Chinese Academy of Medical Sciences (No. 2022-RC350-04), the CAMS Innovation Fund for Medical Sciences (Nos. 2021-I2M-1-026, 2022-I2M-2-002-2, and 2021-I2M-3-001), and Beijing Nova Program to K.H. This work was also supported by the National Natural Science Foundation of China (Nos. 82372002, 62371051, 61971049, and 22278037), the

Projects of International Cooperation and Exchanges NSFC (No. 62211530446), and the Discipline construction of material science and engineering (No. 21090123007).

Disclosure of conflict of interest

None.

Address correspondence to: Ruping Liu, Beijing Engineering Research Center of Printed Electronics, School of Printing and Packaging Engineering, Beijing Institute of Graphic Communication, Beijing 102600, China. Tel: +86-15911058136; E-mail: liuruping@bigc.edu.cn; Kuan Hu, State Key Laboratory of Bioactive Substance and Function of Natural Medicines, Institute of Materia Medica, Chinese Academy of Medical Sciences and Peking Union Medical College, Beijing 100050, China. Tel: +86-13381066782; E-mail: hukuan@imm.ac.cn

References

[1] Phelps ME, Hoffman EJ, Huang SC and Kuhl DE. ECAT: a new computerized tomographic imaging system for positron-emitting radiopharmaceuticals. J Nucl Med 1978; 19: 635-647.
[2] Cherry SR, Jones T, Karp JS, Qi J, Moses WW and Badawi RD. Total-body PET: maximizing sensitivity to create new opportunities for clinical research and patient care. J Nucl Med 2018; 59: 3-12.
[3] Slart RHJA, Tsoumpas C, Glaudemans AWJM, Noordzij W, Willemsen ATM, Borra RJH, Dierckx RAJO and Lammertsma AA. Long axial field of view PET scanners: a road map to implementation and new possibilities. Eur J Nucl Med Mol Imaging 2021; 48: 4236-4245.
[4] Wagner HN Jr. Clinical PET: its time has come. J Nucl Med 1991; 32: 561-564.
[5] Abdallah YMY. History of medical imaging. Archives of Medicine and Health Sciences 2017; 5: 275.
[6] van der Vos CS, Koopman D, Rijnsdorp S, Arends AJ, Boellaard R, van Dalen JA, Lubberink M, Willemsen ATM and Visser EP. Quantification, improvement, and harmonization of small lesion detection with state-of-the-art PET. Eur J Nucl Med Mol Imaging 2017; 44 Suppl 1: 4-16.
[7] Weber WA. Positron emission tomography as an imaging biomarker. J Clin Oncol 2006; 24: 3282-3292.
[8] Badawi RD, Shi H, Hu P, Chen S, Xu T, Price PM, Ding Y, Spencer BA, Nardo L, Liu W, Bao J, Jones T, Li H and Cherry SR. First human imaging studies with the EXPLORER total-body PET scanner. J Nucl Med 2019; 60: 299-303.
[9] Michael M, Jun Z, Katherine B, Jerome G, Thomas L, Manoj N, Deepa N, Sharon W and Michael K. Characterization of the vereos digital photon counting PET system. J Nucl Med 2015; 56: 434.
[10] Jakoby BW, Bercier Y, Conti M, Casey ME, Bendriem B and Townsend DW. Physical and clinical performance of the mCT time-of-flight PET/CT scanner. Phys Med Biol 2011; 56: 2375.
[11] Biograph Vision Quadra [https://www.siemens-healthineers.com/tr/molecular-imaging/pet-ct/biograph-vision-quadra].
[12] Total-body PET Scanner [https://explorer.ucdavis.edu/].
[13] Cherry SR, Badawi RD, Jones T, Kontos D, Flohr TG and Lo JY. EXPLORER: changing the molecular imaging paradigm with total-body PET/CT (Conference Presentation). In: Medical Imaging 2016. Physics of Medical Imaging; 2016.
[14] Zhang X, Xie Z, Berg E, Judenhofer MS, Liu W, Xu T, Ding Y, Lv Y, Dong Y, Deng Z, Tang S, Shi H, Hu P, Chen S, Bao J, Li H, Zhou J, Wang G, Cherry SR, Badawi RD and Qi J. Total-body dynamic reconstruction and parametric imaging on the uEXPLORER. J Nucl Med 2020; 61: 285-291.
[15] Hioki T, Gholami YH, McKelvey KJ, Aslani A, Marquis H, Eslick EM, Willowson KP, Howell VM and Bailey DL. Overlooked potential of positrons in cancer therapy. Sci Rep 2021; 11: 2475.
[16] Salas JR and Clark PM. Signaling pathways that drive (18)F-FDG accumulation in cancer. J Nucl Med 2022; 63: 659-663.
[17] Cook GJ, Houston S, Rubens R, Maisey MN and Fogelman I. Detection of bone metastases in breast cancer by 18FDG PET: differing metabolic activity in osteoblastic and osteolytic lesions. J Clin Oncol 1998; 16: 3375-3379.
[18] Truong MT, Erasmus JJ, Munden RF, Marom EM, Sabloff BS, Gladish GW, Podoloff DA and Macapinlac HA. Focal FDG uptake in mediastinal brown fat mimicking malignancy: a potential pitfall resolved on PET/CT. AJR Am J Roentgenol 2004; 183: 1127-32.
[19] An YS, Yoon JK, Lee MH, Joh CW and Yoon SN. False negative F-18 FDG PET/CT in nonsmall cell lung cancer bone metastases. Clin Nucl Med 2005; 30: 203-204.
[20] Zhang J, Ni Y and Dong A. Infected mediastinal bronchogenic cyst mimicking malignancy on FDG PET/CT. Clin Nucl Med 2020; 45: 172-173.
[21] Saboury B, Morris MA, Nikpanah M, Werner TJ, Jones EC and Alavi A. Reinventing molecular imaging with total-body PET, part II: clinical applications. PET Clin 2020; 15: 463-475.
[22] Cherry SR, Badawi RD, Karp JS, Moses WW, Price P and Jones T. Total-body imaging: transforming the role of positron emission tomography. Sci Transl Med 2017; 9: eaaf6169.

[23] Tan H, Sui X, Yin H, Yu H, Gu Y, Chen S, Hu P, Mao W and Shi H. Total-body PET/CT using half-dose FDG and compared with conventional PET/CT using full-dose FDG in lung cancer. Eur J Nucl Med Mol Imaging 2021; 48: 1966-1975.

[24] Sachpekidis C, Pan L, Kopp-Schneider A, Weru V, Hassel JC and Dimitrakopoulou-Strauss A. Application of the long axial field-of-view PET/CT with low-dose [(18)F]FDG in melanoma. Eur J Nucl Med Mol Imaging 2023; 50: 1158-1167.

[25] Hu Y, Liu G, Yu H, Gu J and Shi H. Diagnostic performance of total-body (18)F-FDG PET/CT with fast 2-min acquisition for liver tumours: comparison with conventional PET/CT. Eur J Nucl Med Mol Imaging 2022; 49: 3538-3546.

[26] Hu Y, Liu G, Yu H, Wang Y, Li C, Tan H, Chen S, Gu J and Shi H. Feasibility of acquisitions using total-body PET/CT with an ultra-low (18)F-FDG activity. J Nucl Med 2022; 63: 959-965.

[27] Zhang Y, Hu P, He Y, Yu H, Tan H, Liu G, Gu J and Shi H. Ultrafast 30-s total-body PET/CT scan: a preliminary study. Eur J Nucl Med Mol Imaging 2022; 49: 2504-2513.

[28] Henrich TJ, Jones T, Beckford-Vera D, Price PM and VanBrocklin HF. Total-body PET imaging in infectious diseases. PET Clin 2021; 16: 89-97.

[29] van Rijsewijk ND, van Leer B, Ivashchenko OV, Scholvinck EH, van den Heuvel F, van Snick JH, Slart RHJA, Noordzij W and Glaudemans AWJM. Ultra-low dose infection imaging of a newborn without sedation using long axial field-of-view PET/CT. Eur J Nucl Med Mol Imaging 2023; 50: 622-623.

[30] Chawla SC, Federman N, Zhang D, Nagata K, Nuthakki S, McNitt-Gray M and Boechat MI. Estimated cumulative radiation dose from PET/CT in children with malignancies: a 5-year retrospective review. Pediatr Radiol 2010; 40: 681-686.

[31] Chen W, Liu L, Li Y, Li S, Li Z, Zhang W, Zhang X, Wu R, Hu D, Sun H, Zhou Y, Fan W, Zhao Y, Zhang Y and Hu Y. Evaluation of pediatric malignancies using total-body PET/CT with half-dose [(18)F]-FDG. Eur J Nucl Med Mol Imaging 2022; 49: 4145-4155.

[32] Reichkendler M, Andersen FL, Borgwardt L, Nygaard U, Albrecht-Beste E, Andersen KF, Ljunggren A, Abrahamsen N, Loft A, Højgaard L and Fischer BM. A long axial field of view enables PET/CT in toddler without sedation. J Nucl Med 2022; 63: 1962.

[33] Zhao YM, Li YH, Chen T, Zhang WG, Wang LH, Feng J, Li C, Zhang X, Fan W and Hu YY. Image quality and lesion detectability in low-dose pediatric (18)F-FDG scans using total-body PET/CT. Eur J Nucl Med Mol Imaging 2021; 48: 3378-3385.

[34] Li Y, Wang J, Hu J, Jia J, Sun H, Zhao Y and Hu Y. PET/CT scan without sedation: how to use total-body PET/CT to salvage child's involuntary movement? Eur J Nucl Med Mol Imaging 2023; 50: 2912-2913.

[35] Schwarzenboeck SM, Rauscher I, Bluemel C, Fendler WP, Rowe SP, Pomper MG, Afshar-Oromieh A, Herrmann K and Eiber M. PSMA ligands for PET imaging of prostate cancer. J Nucl Med 2017; 58: 1545-1552.

[36] Torre LA, Siegel RL, Ward EM and Jemal A. Global cancer incidence and mortality rates and trends--an update. Cancer Epidemiol Biomarkers Prev 2016; 25: 16-27.

[37] Eder M, Schafer M, Bauder-Wust U, Hull WE, Wangler C, Mier W, Haberkorn U and Eisenhut M. 68Ga-complex lipophilicity and the targeting property of a urea-based PSMA inhibitor for PET imaging. Bioconjug Chem 2012; 23: 688-697.

[38] Hope TA, Aggarwal R, Chee B, Tao D, Greene KL, Cooperberg MR, Feng F, Chang A, Ryan CJ, Small EJ and Carroll PR. Impact of (68)Ga-PSMA-11 PET on management in patients with biochemically recurrent prostate cancer. J Nucl Med 2017; 58: 1956-1961.

[39] Ferraro DA, Garcia Schuler HI, Muehlematter UJ, Eberli D, Muller J, Muller A, Gablinger R, Kranzbuhler H, Omlin A, Kaufmann PA, Hermanns T and Burger IA. Impact of (68)Ga-PSMA-11 PET staging on clinical decision-making in patients with intermediate or high-risk prostate cancer. Eur J Nucl Med Mol Imaging 2020; 47: 652-664.

[40] Zhao Q, Yang B, Dong A and Zuo C. 68Ga-PSMA-11 PET/CT in isolated bilateral adrenal metastases from prostate adenocarcinoma. Clin Nucl Med 2022; 47: e101-e102.

[41] Giesel FL, Hadaschik B, Cardinale J, Radtke J, Vinsensia M, Lehnert W, Kesch C, Tolstov Y, Singer S, Grabe N, Duensing S, Schafer M, Neels OC, Mier W, Haberkorn U, Kopka K and Kratochwil C. F-18 labelled PSMA-1007: biodistribution, radiation dosimetry and histopathological validation of tumor lesions in prostate cancer patients. Eur J Nucl Med Mol Imaging 2017; 44: 678-688.

[42] Sharma P, Watts A and Singh H. Comparison of internal dosimetry of 18 F-PSMA-1007 and 68 Ga-PSMA-11-HBED-CC. Clin Nucl Med 2022; 47: 948-953.

[43] Rahbar K, Afshar-Oromieh A, Seifert R, Wagner S, Schafers M, Bogemann M and Weckesser M. Diagnostic performance of (18)F-PSMA-1007 PET/CT in patients with biochemical recurrent prostate cancer. Eur J Nucl Med Mol Imaging 2018; 45: 2055-2061.

[44] Tragardh E, Simoulis A, Bjartell A and Jogi J. Tumor detection of (18)F-PSMA-1007 in the

prostate gland in patients with prostate cancer using prostatectomy specimens as reference method. J Nucl Med 2021; 62: 1735-1740.
[45] Alberts I, Hunermund JN, Prenosil G, Mingels C, Bohn KP, Viscione M, Sari H, Vollnberg B, Shi K, Afshar-Oromieh A and Rominger A. Clinical performance of long axial field of view PET/CT: a head-to-head intra-individual comparison of the Biograph Vision Quadra with the Biograph Vision PET/CT. Eur J Nucl Med Mol Imaging 2021; 48: 2395-2404.
[46] Afshar-Oromieh A, Hetzheim H, Kubler W, Kratochwil C, Giesel FL, Hope TA, Eder M, Eisenhut M, Kopka K and Haberkorn U. Radiation dosimetry of (68)Ga-PSMA-11 (HBED-CC) and preliminary evaluation of optimal imaging timing. Eur J Nucl Med Mol Imaging 2016; 43: 1611-1620.
[47] Afshar-Oromieh A, Malcher A, Eder M, Eisenhut M, Linhart HG, Hadaschik BA, Holland-Letz T, Giesel FL, Kratochwil C, Haufe S, Haberkorn U and Zechmann CM. PET imaging with a [68Ga] gallium-labelled PSMA ligand for the diagnosis of prostate cancer: biodistribution in humans and first evaluation of tumour lesions. Eur J Nucl Med Mol Imaging 2013; 40: 486-495.
[48] Fendler WP, Eiber M, Beheshti M, Bomanji J, Ceci F, Cho S, Giesel F, Haberkorn U, Hope TA, Kopka K, Krause BJ, Mottaghy FM, Schoder H, Sunderland J, Wan S, Wester HJ, Fanti S and Herrmann K. (68)Ga-PSMA PET/CT: Joint EANM and SNMMI procedure guideline for prostate cancer imaging: version 1.0. Eur J Nucl Med Mol Imaging 2017; 44: 1014-1024.
[49] Alberts I, Prenosil G, Mingels C, Bohn KP, Viscione M, Sari H, Rominger A and Afshar-Oromieh A. Feasibility of late acquisition [68Ga] Ga-PSMA-11 PET/CT using a long axial field-of-view PET/CT scanner for the diagnosis of recurrent prostate cancer-first clinical experiences. Eur J Nucl Med Mol Imaging 2021; 48: 4456-4462.
[50] Wen J, Zhu Y, Li L, Liu J, Chen Y and Chen R. Determination of optimal (68) Ga-PSMA PET/CT imaging time in prostate cancers by total-body dynamic PET/CT. Eur J Nucl Med Mol Imaging 2022; 49: 2086-2095.
[51] Hofman MS, Violet J, Hicks RJ, Ferdinandus J, Thang SP, Akhurst T, Iravani A, Kong G, Ravi Kumar A, Murphy DG, Eu P, Jackson P, Scalzo M, Williams SG and Sandhu S. [(177)Lu]-PSMA-617 radionuclide treatment in patients with metastatic castration-resistant prostate cancer (LuPSMA trial): a single-centre, single-arm, phase 2 study. Lancet Oncol 2018; 19: 825-833.
[52] Alberts I, Schepers R, Zeimpekis K, Sari H, Rominger A and Afshar-Oromieh A. Combined [68Ga]Ga-PSMA-11 and low-dose 2-[18F]FDG PET/CT using a long-axial field of view scanner for patients referred for [177Lu]-PSMA-radioligand therapy. Eur J Nucl Med Mol Imaging 2023; 50: 951-956.
[53] Rowe SP, Macura KJ, Mena E, Blackford AL, Nadal R, Antonarakis ES, Eisenberger M, Carducci M, Fan H, Dannals RF, Chen Y, Mease RC, Szabo Z, Pomper MG and Cho SY. PSMA-based [(18)F]DCFPyL PET/CT is superior to conventional imaging for lesion detection in patients with metastatic prostate cancer. Mol Imaging Biol 2016; 18: 411-419.
[54] Zia NA, Cullinane C, Van Zuylekom JK, Waldeck K, McInnes LE, Buncic G, Haskali MB, Roselt PD, Hicks RJ and Donnelly PS. A bivalent inhibitor of prostate specific membrane antigen radiolabeled with copper-64 with high tumor uptake and retention. Angew Chem Int Ed Engl 2019; 58: 14991-14994.
[55] Ingbritsen J, Callahan J, Morgan H and Hicks RJ. Multiple angiolipomas visualized by dynamic and delayed "total-body" [(18)F]-DCFPyL and [(64)Cu]-SARbisPSMA PET/CT. Eur J Nucl Med Mol Imaging 2023; [Epub ahead of print].
[56] Reubi JC and Waser B. Concomitant expression of several peptide receptors in neuroendocrine tumours: molecular basis for in vivo multireceptor tumour targeting. Eur J Nucl Med Mol Imaging 2003; 30: 781-793.
[57] Reubi JC, Schär JC, Waser B, Wenger S, Heppeler A, Schmitt JS and Mäcke HR. Affinity profiles for human somatostatin receptor subtypes SST1-SST5 of somatostatin radiotracers selected for scintigraphic and radiotherapeutic use. Eur J Nucl Med 2000; 27: 273-282
[58] Bozkurt MF, Virgolini I, Balogova S, Beheshti M, Rubello D, Decristoforo C, Ambrosini V, Kjaer A, Delgado-Bolton R, Kunikowska J, Oyen WJG, Chiti A, Giammarile F, Sundin A and Fanti S. Guideline for PET/CT imaging of neuroendocrine neoplasms with (68)Ga-DOTA-conjugated somatostatin receptor targeting peptides and (18)F-DOPA. Eur J Nucl Med Mol Imaging 2017; 44: 1588-1601.
[59] Zhang YQ, Hu PC, Wu RZ, Gu YS, Chen SG, Yu HJ, Wang XQ, Song J and Shi HC. The image quality, lesion detectability, and acquisition time of (18)F-FDG total-body PET/CT in oncological patients. Eur J Nucl Med Mol Imaging 2020; 47: 2507-2515.
[60] Xiao J, Yu H, Yin H, Liu G, Hu Y, Qinyu L, Yanzhao Z, Zhang Y, Hu P, Cheng D and Shi H. Feasibility of low-dose 68Ga-DOTATATE with short acquisition time using total-body PET/CT in patients with neuroendocrine tumor. 2021.
[61] Challita-Eid PM, Satpayev D, Yang P, An Z, Morrison K, Shostak Y, Raitano A, Nadell R, Liu W, Lortie DR, Capo L, Verlinsky A, Leavitt M, Malik F, Avina H, Guevara CI, Dinh N, Karki S, Anand BS, Pereira DS, Joseph IB, Donate F, Morrison

K and Stover DR. Enfortumab vedotin antibody-drug conjugate targeting Nectin-4 is a highly potent therapeutic agent in multiple preclinical cancer models. Cancer Res 2016; 76: 3003-3013.
[62] Heath EI and Rosenberg JE. The biology and rationale of targeting nectin-4 in urothelial carcinoma. Nat Rev Urol 2021; 18: 93-103.
[63] Duan X, Xia L, Zhang Z, Ren Y, Pomper MG, Rowe SP, Li X, Li N, Zhang N, Zhu H, Yang Z, Sheng X and Yang X. First-in-human study of the radioligand 68Ga-N188 targeting nectin-4 for PET/CT imaging of advanced urothelial carcinoma. Clin Cancer Res 2023; 29: 3395-3407.
[64] Wang LC, Lo A, Scholler J, Sun J, Majumdar RS, Kapoor V, Antzis M, Cotner CE, Johnson LA, Durham AC, Solomides CC, June CH, Pure E and Albelda SM. Targeting fibroblast activation protein in tumor stroma with chimeric antigen receptor T cells can inhibit tumor growth and augment host immunity without severe toxicity. Cancer Immunol Res 2014; 2: 154-166.
[65] Zboralski D, Osterkamp F, Christensen E, Bredenbeck A, Schumann A, Hoehne A, Schneider E, Paschke M, Ungewiss J, Haase C, Robillard L, Simmons AD, Harding TC and Nguyen M. Fibroblast activation protein targeted radiotherapy induces an immunogenic tumor microenvironment and enhances the efficacy of PD-1 immune checkpoint inhibition. Eur J Nucl Med Mol Imaging 2023; 50: 2621-2635.
[66] Rohrich M, Naumann P, Giesel FL, Choyke PL, Staudinger F, Wefers A, Liew DP, Kratochwil C, Rathke H, Liermann J, Herfarth K, Jager D, Debus J, Haberkorn U, Lang M and Koerber SA. Impact of (68)Ga-FAPI PET/CT imaging on the therapeutic management of primary and recurrent pancreatic ductal adenocarcinomas. J Nucl Med 2021; 62: 779-786.
[67] Lindner T, Loktev A, Altmann A, Giesel F, Kratochwil C, Debus J, Jager D, Mier W and Haberkorn U. Development of quinoline-based theranostic ligands for the targeting of fibroblast activation protein. J Nucl Med 2018; 59: 1415-1422.
[68] Zhang X, Song W, Qin C, Liu F and Lan X. Non-malignant findings of focal (68)Ga-FAPI-04 uptake in pancreas. Eur J Nucl Med Mol Imaging 2021; 48: 2635-2641.
[69] Lin R, Lin Z, Zhang J, Yao S and Miao W. Increased 68Ga-FAPI-04 uptake in schmorl node in a patient with gastric cancer. Clin Nucl Med 2021; 46: 700-702.
[70] Chen R, Yang X, Ng YL, Yu X, Huo Y, Xiao X, Zhang C, Chen Y, Zheng C, Li L, Huang G, Zhou Y and Liu J. First total-body kinetic modeling and parametric imaging of dynamic (68)Ga-FAPI-04 PET in pancreatic and gastric cancer. J Nucl Med 2023; 64: 960-967.
[71] Jia C, Wu M, Yen TC, Li Y and Cui R. Complementary utility of dopamine transporter and Tau PET imaging in the diagnosis of progressive supranuclear palsy: a case report. Clin Nucl Med 2022; 47: 336-338.
[72] Xin M, Li L, Wang C, Shao H, Liu J and Zhang C. Pilot study on (11)C-CFT dynamic imaging using total-body PET/CT: biodistribution and radiation dosimetry in Parkinson's disease. Front Neurol 2023; 14: 1153779.
[73] Pandit-Taskar N, Postow MA, Hellmann MD, Harding JJ, Barker CA, O'Donoghue JA, Ziolkowska M, Ruan S, Lyashchenko SK, Tsai F, Farwell M, Mitchell TC, Korn R, Le W, Lewis JS, Weber WA, Behera D, Wilson I, Gordon M, Wu AM and Wolchok JD. First-in-humans imaging with (89)Zr-Df-IAB22M2C anti-CD8 minibody in patients with solid malignancies: preliminary pharmacokinetics, biodistribution, and lesion targeting. J Nucl Med 2020; 61: 512-519.
[74] Niemeijer AN, Leung D, Huisman MC, Bahce I, Hoekstra OS, van Dongen GAMS, Boellaard R, Du S, Hayes W, Smith R, Windhorst AD, Hendrikse NH, Poot A, Vugts DJ, Thunnissen E, Morin P, Lipovsek D, Donnelly DJ, Bonacorsi SJ, Velasquez LM, de Gruijl TD, Smit EF and de Langen AJ. Whole body PD-1 and PD-L1 positron emission tomography in patients with non-small-cell lung cancer. Nat Commun 2018; 9: 4664.
[75] Bensch F, van der Veen EL, Lub-de Hooge MN, Jorritsma-Smit A, Boellaard R, Kok IC, Oosting SF, Schroder CP, Hiltermann TJN, van der Wekken AJ, Groen HJM, Kwee TC, Elias SG, Gietema JA, Bohorquez SS, de Crespigny A, Williams SP, Mancao C, Brouwers AH, Fine BM and de Vries EGE. (89)Zr-atezolizumab imaging as a non-invasive approach to assess clinical response to PD-L1 blockade in cancer. Nat Med 2018; 24: 1852-1858.
[76] Brouwers AH, van Sluis J, van Snick JH, Schroder CP, Baas IO, Boellaard R, Glaudemans AWJM, Borra RJH, Lammertsma AA, Dierckx RAJO and Tsoumpas C. First-time imaging of [(89)Zr]trastuzumab in breast cancer using a long axial field-of-view PET/CT scanner. Eur J Nucl Med Mol Imaging 2022; 49: 3593-3595.
[77] Sun J, Huangfu Z, Yang J, Wang G, Hu K, Gao M and Zhong Z. Imaging-guided targeted radionuclide tumor therapy: from concept to clinical translation. Adv Drug Deliv Rev 2022; 190: 114538.
[78] Berg E, Gill H, Marik J, Ogasawara A, Williams S, van Dongen G, Vugts D, Cherry SR and Tarantal AF. Total-body PET and highly stable chelators together enable meaningful (89)Zr-antibody PET studies up to 30 days after injection. J Nucl Med 2020; 61: 453-460.